

Attraction Controls the Inversion of Order by Disorder in Buckled Colloidal Monolayers

Fabio Leoni and Yair Shokef

School of Mechanical Engineering and Sackler Center for Computational Molecular and Materials Science, Tel-Aviv University, Tel-Aviv 69978, Israel

Entropy generates stripe patterns in buckled colloidal monolayers. The Ising antiferromagnet on a deformable triangular lattice displays the same ground state as this colloidal system, but it remains unclear if ordering in the two systems is driven by the same geometric mechanism. By a real-space expansion we find that for buckled colloids bent stripes constitute the stable phase, whereas in the Ising antiferromagnet straight stripes are favored. For generic pair potentials we show that attraction governs this selection mechanism, in a manner that is linked to local packing considerations. This supports the geometric origin of entropy in jammed sphere packings.

Geometrically-frustrated systems cannot satisfy all local constraints and thus remain disordered down to zero temperature [1]. Subtle effects such as boundary conditions, lattice distortions, and higher-order or long-range interactions can remove the degeneracy and lead to an ordered ground-state. Alternatively, if entropy of fluctuations about each ground-state configuration slightly varies, then the configuration with the highest entropy [2] will be thermodynamically selected in an effect termed order by disorder [3–5].

Recently, frustration typical of antiferromagnetic spin models has been studied in mesoscopic systems, composed of magnetic islands [6, 7], colloidal spheres [8–11] or elastic beams [12, 13]. The ability to visualize and manipulate individual particles is also very useful to study glass formers [14], crystals, and gels [15]. For colloidal spheres confined between parallel walls, varying density and plate separation (from one to two colloid diameters) a first-order fluid freezing transition and discontinuous phase transitions between layered, buckled and rhombic crystal structures occur [16, 17]. When the density approaches close packing, the monolayer buckles out of its plane and neighboring spheres tend to touch opposite walls, giving rise to effective antiferromagnetic interactions [18] and to glassy dynamics [19]. Multiple states with the same maximal density are obtained by alternating straight stripes of up and down spheres (Fig. 1a) or by any set of zigzagging stripes (Fig. 1b).

Slightly below this close-packing density it is difficult to find analytic results regarding the thermodynamically stable phase. Instead, one can study an antiferromagnetic Ising model on a deformable triangular lattice which exhibits a highly-degenerate ground-state of randomly-zigzagging stripes at $T = 0$, corresponding to the close-packed density (at $\rho = \rho_c$) in the colloidal system. The degeneracy of the ground state is removed for $T > 0$ through an order-by-disorder effect: the thermodynamically stable phase is set by differences in entropy of fluctuations around the different ground-state configurations. In this model, fluctuations around the ground state are harmonic, thus the phonon spectrum may be calculated

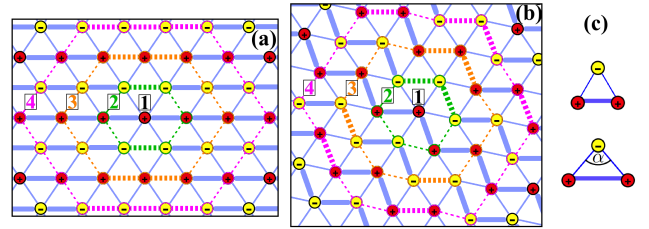


FIG. 1. (a) Straight and (b) bent (maximally zigzagging) configurations. Shells of free spins are enumerated and connected by dashed lines of the same color. Thicker lines correspond to frustrated bonds connecting spins (or spheres) at the same state. (c) rigid equilateral (top) and deformed isosceles (bottom) plaquette of the triangular lattice.

and from it one finds that straight stripes are selected [20]. While this approach allows to compute the entropy of the system, it is unclear what is the mechanism behind the entropy selection of the ground state and what is the full connection between this model and the confined colloidal system.

In this Letter we compute in real-space coordinates the entropies of the competing stripe configurations both in the deformable Ising antiferromagnet and in the confined colloidal system for colloids modeled with different pair potentials. To compute the entropy of colloids modeled as hard-spheres we develop a geometric approach related to that employed to estimate the free volume of fcc vs hcp structures [21–23]. While one could expect that repulsion would flatten out things and give a preference for straight-stripe patterns, we find that generic repulsive potentials give preference for bent stripes. In the Ising antiferromagnet straight stripes are favored, since there attraction is included. This implies that attraction is responsible for flipping the sign of the order-by-disorder effect in this system.

Ising Model: Each spin is linked to six neighbors by harmonic springs to form a deformable triangular lattice, with the Hamiltonian given by the sum over all nearest-neighbor pairs $\mathcal{H} = \sum_{\langle ij \rangle} \left[(1 - \epsilon \delta r_{ij}) J \sigma_i \sigma_j + \frac{K}{2} \delta r_{ij}^2 \right]$.

$\sigma_i = \pm 1$ and $\delta r_{ij} = |\vec{r}_i - \vec{r}_j| - a$ are the spin and relative position variables, respectively, $J > 0$ is the antiferromagnetic interaction strength, a is the relaxed spring length, $\epsilon > 0$ is the rate at which the antiferromagnetic interaction decreases linearly with distance, and K the spring stiffness. In the ground state, each plaquette deforms to an isosceles triangle with two shorter satisfied bonds and one longer frustrated bond (Fig. 1c). Minimizing energy with respect to the head angle α of these isosceles triangles relates α to the dimensionless ratio $b = J\epsilon/Ka > 0$ of the magnetoelastic interaction to the lattice rigidity [20]. At sufficiently low temperature (i.e. $k_B T \ll J$), spins cannot flip and the Hamiltonian for straight and bent stripes configurations can be expanded around mechanical equilibrium: $\mathcal{H} = K \sum_{m,n} A_{m,n} q_m q_n$. $\{q\} = \{u, v\}$ represents small displacements about the equilibrium position of every spin, namely, m and n run from 1 to $2N$, where N is the number of spins in the lattice. Since b is set by α , the dimensionless matrix A depends only on the deformation angle α and on the zigzagging stripe realization $\{\sigma_i\}$. The canonical partition function (up to multiplicative constants) reads

$$Z = \int \exp(-\beta K \sum_{m,n} A_{m,n} q_m q_n) d\{q\} = \left(\frac{\pi}{\beta K}\right)^N \|A\|^{-1/2} \quad (1)$$

where $\beta = 1/T$, $\|A\|$ is the determinant of A and we measure temperature in units in which Boltzmann's constant is one. The entropy reads

$$S = -\frac{\beta}{Z} \left(\frac{\partial Z}{\partial \beta}\right) + \ln Z = N \left[1 + \ln \left(\frac{\pi}{K\beta}\right)\right] - \frac{1}{2} \ln(\|A\|). \quad (2)$$

Computing the entropy of the system considering some particles free to move and all others fixed in their ground-state positions enables us to analyze the contribution to the entropy coming from a specific subset of particles. This requires to find for A a recursive relation which can be extended to an increasing number n of free particles. To this end we consider n_s shells of particles for straight (Fig. 1a) and bent (Fig. 1b) configurations. These numbers are related by $n = 1 + 3n_s(n_s - 1)$. In Fig. 2a we show that the entropy difference per particle $\Delta s = (S_{\text{straight}} - S_{\text{bent}})/n$ between straight and bent configurations as obtained from our shell expansion method converges to the exact phonon solution [20]. *Considering only one particle free to move already gives a qualitative picture of the entropy difference.* For small angles ($60^\circ < \alpha < 130^\circ$) the curves slowly approach the phonon solution, whereas for large angles ($130^\circ < \alpha < 180^\circ$) they decrease fast up to $n_s \approx 7$, and then, further increasing n_s , the two minima tend to merge very slowly to one minimum and for $n_s > 20$ the curves invert the decreasing trend to start to increase and slowly approach the phonon solution.

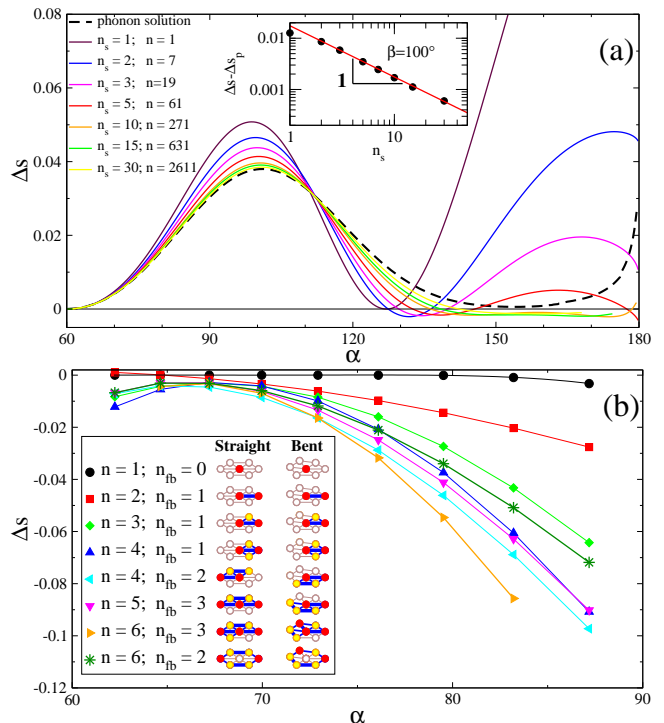


FIG. 2. Entropy difference per particle between straight and bent configurations vs deformation angle α . (a) Ising antiferromagnet: Results with different numbers or free spins converge to the phonon solution Δs_p . Inset: distance between Δs and Δs_p at $\alpha = 100^\circ$ vs n_s . (b) Hard-sphere monolayer: number of free spheres n and number of frustrated bonds n_{fb} indicated in the legend: red (up) and yellow (down) particles are allowed to move, empty circles denote particles kept fixed. Thicker blue lines are frustrated bonds. The line for $n = 1$ is an analytic expression, while the lines for other n are guides to the eye.

Buckled hard spheres: Colloidal particles with short-range repulsion are usually theoretically approximated as hard spheres [8, 24]. For hard spheres, momentum variables are irrelevant and, except for an additive constant, the entropy reads $S_N = \ln(V_N)$ where V_N is the $3N$ -dimensional phase-space volume available to the centers of the N spheres.

We compute the entropy of the straight and bent close-packed configurations (see Fig. 3) by directly calculating their phase-space volume. To obtain the entropy of fluctuations about the close-packed state we slightly decrease the density below close-packing by reducing the radius c of all spheres by $\delta \ll c$ [25]. In this way spheres have room to move, and following a free-sphere expansion [21], we allow an increasing number n of contiguous spheres to move while the centers of the other $N - n$ remain fixed in their close-packed positions.

The shrinking of spheres, $c \rightarrow c - \delta$, implies the scaling $V_n \sim \delta^{3n}$. V_n is the phase space volume associated to the n spheres free to move, described by a $3n$ -

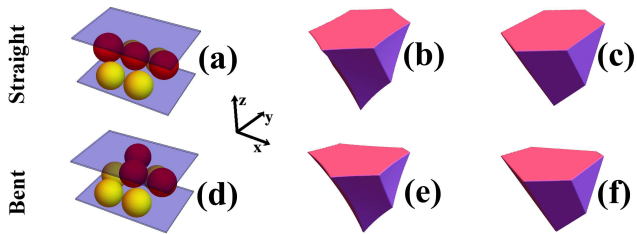


FIG. 3. Straight (a-c) and bent (d-f) configurations. (a,d) yellow (red) spheres are in contact with the bottom (top) plane. Phase-space volume of one hard sphere free to move given by the 3-dimensional volume V_1 , considering curved (b,e) and flat (c,f) surfaces. Here $\alpha = 70^\circ$ and $\delta/c = 0.08$ to emphasize the difference between curved and flat surfaces.

dimensional volume delimited by curved surfaces. Considering one sphere free to move, the surface of the free volume V_1 is described by rolling the free sphere in all possible ways over its six neighbor spheres and over one confining wall (Fig. 3b,e). For $\delta \ll c$ it is possible to neglect the curvature of the surfaces [21–23], thus obtaining linear restrictions (planes) (Fig. 3c,f), and then to compute V_1 as a 3-dimensional polyhedron, and for n free spheres to similarly compute V_n as a $3n$ -dimensional polytope [25, 26]. V_1 is given by the Voronoi cell associated to the center of the free sphere scaled by 2δ and the entropy of straight and bent configurations at this level coincide (as for fcc and hcp), but here only up to $\alpha^* = 2 \arctan\left(\sqrt{8/(7 + \sqrt{33})}\right) \simeq 77^\circ$ [25], after which bent-stripe entropy is higher than straight-stripe entropy (Fig. 2b). For bent stripes with $\alpha > \alpha^*$ when the free sphere is close to the top wall the condition coming from one of the bottom spheres becomes irrelevant [25]. Therefore, *in confinement already with one free sphere, there are local configurations of a collectively jammed state [27] with the same free energy at close packing which differ in their local stability for slightly decreasing density.* We will show that this is valid also for larger n .

For $n = 2$, the free volume can be computed through a 6-dimensional integral [23]. Because the correlated motion of the free spheres, to find the free volume for $n > 2$ requires more sophisticated tools. For that we use a modified version of the Lasserre method [28, 29] implemented in the VINCI code [30]. We calculated the phase-space volumes V_n for straight and bent configurations up to $n = 6$ spheres that are free to move corresponding to 18-dimensional polytopes [25]. Figure 2b shows the entropy difference per particle for different sets of n contiguous spheres free to move with $\delta/c = 0.001$ (considering smaller values of δ did not change the result) with the same number of frustrated bonds n_{fb} . *We find that bent stripes are thermodynamically stable, which is the opposite from the Ising antiferromagnet result shown in Fig. 2a.* Increasing the number of free

spheres, the entropy difference increases, especially for large angles. From existing experiments on colloidal monolayers [8, 19, 31] it is hard to conclude if the ground state has a preference for straight or bent stripes because the system has to be annealed very slowly [18, 20]. From the experimental interparticle potential of NIPA colloids [24] it is possible to see that a simple correction to the hard sphere potential can be described by a decreasing exponential. However, this potential is in the same “quasi-universality” class with hard spheres [32], hence no qualitative change in the results is expected. Softer interactions such as the square-shoulder with a hard core surrounded by a soft corona, does not change the preference for bent over straight stripes [25].

Attraction: Elasticity in the Ising model includes attraction and repulsion which contribute equally, while hard- or soft-sphere interactions used to model colloids are purely repulsive. Adding attraction to repulsive colloids can induce a clustering phase [33], a solid-solid transition [34], a glass-glass transition [35] and many other phenomena [14]. To investigate the role of attraction in the entropy selection of the ground state, we first consider a system of particles in the same straight and bent positions as the buckled colloidal system with particles interacting either through a harmonic potential $U(\zeta) = U_0\zeta^2$ or through a purely repulsive harmonic potential $U_r(\zeta) = U_0\zeta^2 \cdot \theta(\zeta)$ where $\theta(\zeta)$ is the Heaviside step function, $\zeta = (dr_0 - dr)/(2\delta)$ and U_0 sets the energy scale. $dr_0 = 2c$ and $dr^2 = dr_0^2 + du^2 + dv^2 + dw^2$ with $\{u, v, w\}$ the displacement around the equilibrium position. The entropy of straight and bent configurations for particles interacting through $U(\zeta)$ can be exactly calculated [25], while for $U_r(\zeta)$ we use the canonical partition function obtained by numerical integration [25]. From Fig. 4a,b, which shows Δs for $U(\zeta)$ and $U_r(\zeta)$ respectively, we see that the harmonic potential $U(\zeta)$ gives a result qualitatively similar to that of the Ising antiferromagnet (Fig. 2a) with a preference for straight stripes. On the other hand, *considering only the repulsive part of the harmonic potential, using $U_r(\zeta)$, changes the preference to bent stripes, as we found for hard spheres (Fig. 2b).*

Considering the generalized repulsive potential $U_r^\gamma(\zeta) = U_r^0\zeta^\gamma \cdot \theta(\zeta)$, which reduces to the repulsive harmonic potential for $\gamma = 2$ and gives hard spheres of diameter $2(c - \delta)$ for $\gamma \rightarrow \infty$ [36], for increasing the constant γ , Δs for one particle free to move slowly approaches the hard-sphere result and always exhibits a preference for bent stripes, implying that attraction is responsible for the inversion of Δs [25]. More generally we consider an asymmetric power-law potential $U_{asy}(\zeta) = U_r^0\zeta^{\gamma_r}\theta(\zeta) + U_a^0(-\zeta)^{\gamma_a}\theta(-\zeta)$ through which we can tune both repulsion and attraction. We find a transition from bent to straight stripes by reducing the attraction, that is for $\gamma_a/\gamma_r = \kappa(\alpha)$ (with $0 < 1/\kappa < 1$) [25] (see Fig. 4c). Note that for small

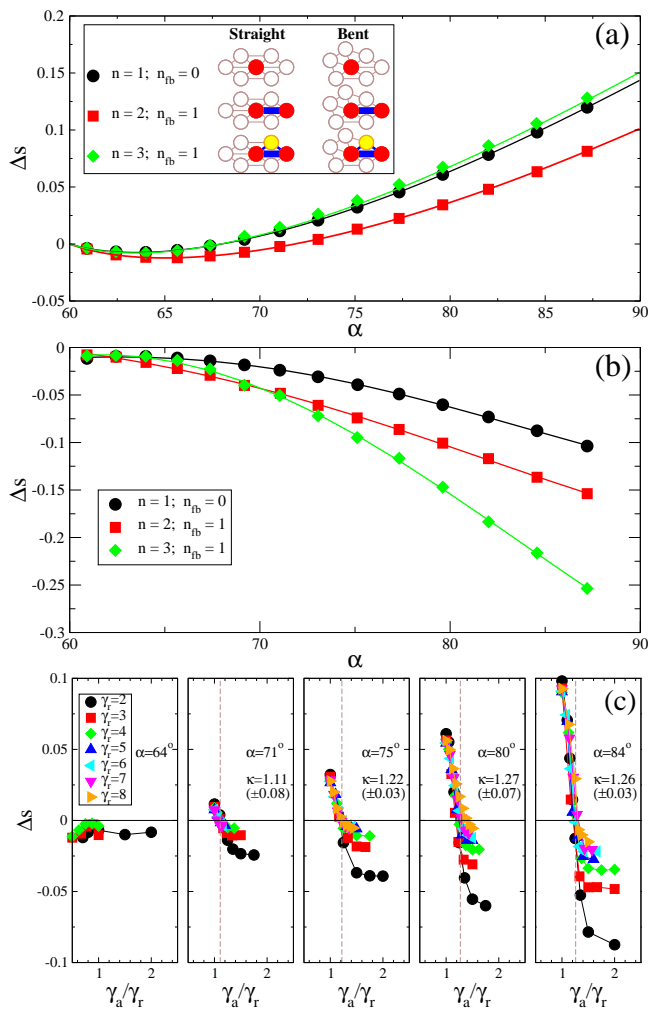


FIG. 4. Entropy difference per particle between straight and bent configurations vs deformation angle α . (a) Harmonic potential $U(\zeta)$. Particles indicated in the legend same as in Fig. 2b. (b) Repulsive harmonic potential $U_r(\zeta)$. (c) Asymmetric potential $U_{\text{asy}}(\zeta)$: Δs vs the ratio γ_a/γ_r for different values of γ_r . The curves are computed for $n = 1$, $U_a^0 = U_r^0$, and the vertical lines indicate $\kappa(\alpha)$.

angles, $\Delta s < 0$ also for the symmetric case. This is closely related to the geometric origin of the preference for bent over straight stripes for $\alpha > \alpha^*$ for one free hard sphere; considering a symmetric potential, like the harmonic potential, means to always include the contribution from all neighbors for all angles, while considering a purely repulsive potential (or properly reducing the attraction) allows to disregard (or reduce enough) the contribution from one of the bottom spheres for certain heights due to the same geometric reasons as for hard spheres [25]. We conjecture that the same mechanism acts for more than one particle free to move. It would be interesting to experimentally test this effect of attraction and repulsion on the ground state, for example using magnetic colloids [37].

Conclusions: We computed via real-space coordinates the entropies for small fluctuations of the competing stripe configurations both in the deformable Ising antiferromagnet and in the colloidal monolayer for colloids modeled as hard or soft spheres. In the Ising antiferromagnet straight stripes are favored, while for buckled colloids bent stripes are selected. In many compact systems such as fcc and hcp using a harmonic potential or a purely repulsive one doesn't change the result (for example by lattice dynamical theory [38, 39]), yet we found that it is fundamental. We found that attraction influences the ground-state selection mechanism changing the sign of Δs , and related it with local geometric properties. Local geometry plays an important role in jamming [40, 41], even though it cannot give a complete picture [27]. Our results could be useful to understand why some characteristics of the jamming transition are related to local geometric properties such as the mean number of nearest neighbors of Voronoi volumes and mean number of constraints [41]. Indeed, inverting Δs for one free hard sphere corresponds to changing the number of nearest neighbors or the number of constraints. This mechanism is possible for dimensions $d \geq 3$ and it could be related to the upper critical dimension for jamming suggested to be equal to 3 [41]: shrinking spheres in a jammed state by $\delta \ll c$, which is still a jammed state [27], we can conjecture to have many different local configurations with the same density, the entropies of which after shrinking may differ for each one of them. It would be interesting to test the relevance of attraction in other buckled patterns, as for glassy states with numerous coordination polyhedrons [42].

Our results could be relevant to designing colloidal systems and to self-assembly of structures. DNA-coated colloids can be designed by controlling the nucleotide sequences, coating densities and the attractive and repulsive component [43]. Attraction is responsible for self-assembly of nanocrystal superlattices [44]. Predicting spontaneously-formed structures from properties of building blocks is another example of the role played by local geometry [45]. The square lattice with quadratic interactions between next-nearest-neighbour sites can be turned from stable to a highly degenerate zigzag state by tuning the quadratic coefficient from positive to negative [46]. Crucial differences between random spring networks and jammed packings caused by redundant constraints [47] could originate from attraction. It could be interesting to study a possible transition in a network of asymmetric-interacting points from the random spring to the jammed-packing behavior. Finally, it would be interesting to test our theoretical predictions in simulations and try to improve algorithms to find random packings of jammed frictionless hard spheres.

We thank C. Calero, R. Golkov, Y. Han, E. Oğuz, N. Segall, A. Souslov, G. Tarjus and E. Teomy for helpful discussions. This research was supported by the Israel

Science Foundation Grant No. 968/16.

-
- [1] G. Tarjus, S. A. Kivlson, Z. Nussinov, and P. Viot, *J. Phys.: Condens. matter* **17**, R1143 (2005).
- [2] Formally, we should seek the configuration that minimizes free energy rather than for the one that maximizes entropy. However we show that in our case this is equivalent [25].
- [3] M. F. Collins and O. A. Petrenko, *Can. J. Phys.* **75**, 605 (1997).
- [4] F. Wang and A. Vishwanath, *Phys. Rev. Lett.* **100**, 077201 (2008).
- [5] O. A. Starykh, H. Katsura, and L. Balents, *Phys. Rev. B* **82**, 014421 (2010).
- [6] F. Wang, C. Nisoli, R. S. Freitas, J. Li, W. McConville, B. J. Cooley, M. S. Lund, N. Samarth, C. Leighton, V. H. Crespi, and P. Schiffer, *Nature* **439**, 303 (2006).
- [7] C. Nisoli, R. Moessner, and P. Schiffer, *Rev. Mod. Phys.* **85**, 1473 (2013).
- [8] Y. Han, Y. Shokef, A. M. Alsayed, P. Yunker, T. C. Lubensky, and A. G. Yodh, *Nature* **456**, 4857 (2008).
- [9] A. Libál, C. Reichhardt, and C. J. O. Reichhardt, *Phys. Rev. Lett.* **97**, 228302 (2006).
- [10] A. Ortiz-Ambriz and P. Tierno, *Nat. Commun.* **7**, 10575 (2016).
- [11] P. Tierno, *Phys. Rev. Lett.* **116**, 038303 (2016).
- [12] S. Kang, S. Shan, A. Košmrlj, W. Noorduin, S. Shian, J. Weaver, D. Clarke, and K. Bertoldi, *Phys. Rev. Lett.* **112**, 098701 (2014).
- [13] C. Coulais, E. Teomy, K. de Reus, Y. Shokef, and M. van Hecke, *Nature* **535**, 529 (2016).
- [14] S. Gokhale, A. K. Sood, and R. Ganapathy, *Adv. Phys.* **65**, 363 (2016).
- [15] P. J. Lu and D. A. Weitz, *Annu. Rev. Condens. Matter Phys.* **4**, 9.1 (2013).
- [16] M. Schmidt and H. Löwen, *Phys. Rev. Lett.* **76**, 4552 (1996).
- [17] M. Schmidt and H. Löwen, *Phys. Rev. E* **55**, 7228 (1997).
- [18] Y. Shokef and T. C. Lubensky, *Phys. Rev. Lett.* **102**, 048303 (2009).
- [19] Y. Han, private communication.
- [20] Y. Shokef, A. Souslov, and T. C. Lubensky, *Proc. Natl. Acad. Sci. USA* **108**, 11804 (2011).
- [21] W. G. Rudd, Z. W. Salsburg, A. P. Yu, and F. H. Stillinger, *J. Chem. Phys.* **49**, 4857 (1968).
- [22] H. Koch, C. Radin, and L. Sadun, *Phys. Rev. E* **72**, 016708 (2005).
- [23] C. Radin and L. Sadun, *Phys. Rev. Lett.* **94**, 015502 (2005).
- [24] Y. Han, N. Y. Ha, A. M. Alsayed, and A. G. Yodh, *Phys. Rev. E* **77**, 041406 (2008).
- [25] see Supplementary Material.
- [26] B. Büeler, A. Enge, and K. Fukuda, *Exact volume computation for polytopes: A practical study*. In Gil Kalai and Günter M. Ziegler, editors, *Polytopes - Combinatorics and Computation, volume 29 of DMV Seminar, pages 131-154, Basel* (Birkhäuser Verlag, 2000).
- [27] S. Torquato and F. H. Stillinger, *Rev. Mod. Phys.* **82**, 2633 (2010).
- [28] J. B. Lasserre, *J. Optim. Theor. Appl.* **39**, 363 (1983).
- [29] J. B. Lasserre, *Proc. Amer. Math. Soc.* **126**, 2433 (1998).
- [30] <http://www.math.u-bordeaux1.fr/~aenge/index.php?category=so>
- [31] P. J. Yunker, K. Chen, M. D. Gratale, M. A. Lohr, T. Still, and A. G. Yodh, *Rep. Prog. Phys.* **77**, 056601 (2014).
- [32] A. K. Bacher, T. B. Schröder, and J. C. Dyre, *Nat. Commun.* **5**, 5424 (2014).
- [33] P. J. Lu, J. C. Conrad, H. M. Wyss, A. B. Schofield, and D. A. Weitz, *Phys. Rev. Lett.* **96**, 028306 (2006).
- [34] T. van de Laar, R. Higler, K. Schroën, and J. Sprakel, *Sci. Rep.* **6**, 22725 (2016).
- [35] T. Voigtmann, *Europhys. Lett.* **96**, 36006 (2011).
- [36] U_r^γ differs by a numerical prefactor from the commonly-used tunable soft repulsive potential [41, 51, 52], with $dr_0 = \sigma_{ij}$ and $dr = r_{ij}$, and the hard-sphere limit obtained for $\alpha \rightarrow 0$ [51].
- [37] P. Tierno, private communication.
- [38] A. Travesset, *J. Chem. Phys.* **141**, 164501 (2014).
- [39] A. Travesset, private communication.
- [40] S. S. Ashwin and R. K. Bowles, *Phys. Rev. Lett.* **102**, 235701 (2009).
- [41] P. K. Morse and E. I. Corwin, *Phys. Rev. Lett.* **112**, 115701 (2014).
- [42] E. Ma, *Nature Mater.* **14**, 547 (2015).
- [43] S. Angioletti-Uberti, B. M. Mognetti, and D. Frenkel, *Nature Mater.* **11**, 518 (2012).
- [44] X. Ye, J. Chen, M. Engel, J. A. Millan, W. Li, L. Qi, G. Xing, J. E. Collins, C. R. Kagan, J. Li, S. C. Glotzer, and C. B. Murray, *Nature Chem.* **5**, 466 (2013).
- [45] P. F. Damasceno, M. Engel, and S. C. Glotzer, *Science* **337**, 453 (2012).
- [46] X. Mao, A. Souslov, C. I. Mendoza, and T. C. Lubensky, *Nat. Commun.* **6**, 5968 (2015).
- [47] W. G. Ellenbroek, V. F. Hagh, A. Kumar, M. F. Thorpe, and M. van Hecke, *Phys. Rev. Lett.* **114**, 135501 (2015).
- [48] G. Malescio and G. Pellicane, *Nature Mater.* **2**, 97 (2003).
- [49] M. A. Glaser, G. M. Grason, R. D. Kamien, A. Košmrlj, C. D. Santangelo, and P. Zihlerl, *Europhys. Lett.* **78**, 46004 (2007).
- [50] T. Dotera, T. Oshiro, and P. Zihlerl, *Nature* **506**, 208 (2014).
- [51] A. J. Liu and S. R. Nagel, *Annu. Rev. Condens. Matter Phys.* **1**, 347 (2010).
- [52] M. van Hecke, *J. Phys.: Condens. Matter.* **22**, 033101 (2010).

Supplementary Material for “Attraction Controls the Inversion of Order by Disorder in Buckled Colloidal Monolayers”

Fabio Leoni and Yair Shokef

School of Mechanical Engineering and Sackler Center for Computational Molecular and Materials Science, Tel-Aviv University, Tel-Aviv 69978, Israel

In the present supplementary material we provide detailed analytical calculations behind the results presented in the main text of the paper. In Sec. SI we compute the exact free volume available to the center of a sphere in the straight and bent configurations near the close-packing limit from which it is possible to calculate the entropy of such systems. We give also some detail about our implementation of the VINCI code used to compute the volume of high-dimensional polytopes. In Sec. SII we compute the Hamiltonian and entropy of the soft potential model in the small fluctuations approximation for straight and bent configurations. In Sec. SIII we show that the sign of the entropy difference between straight and bent stripes configurations of soft spheres interacting through the square-shoulder repulsive potential is the same as for hard spheres. Finally, in Sec. SIV we define the asymmetric potential and show the transition from straight to bent stripes as the contribution of the attractive component of the potential is reduced compared to the repulsive component.

VOLUME CALCULATION FOR ONE SPHERE FREE TO MOVE

The centers of the spheres of one unit cell in the straight and bent configurations (see Fig. 3a, d) have coordinates $\{(\pm c, \pm d, 0), (0, 0, H), (\pm 2c, 0, H)\}$ and $\{(\pm c, -d, 0), (c, d, 0), (2c, 0, H), (-c(3d^2 - c^2)/(c^2 + d^2), d(3c^2 - d^2)/(c^2 + d^2), 0), (0, 0, H), (-2c(d^2 - c^2)/(c^2 + d^2), 4c^2d/(c^2 + d^2), H)\}$ respectively. The bottom and top confining walls are at $z = -c$ and $z = H + c$ respectively. c is the radius of each sphere. Down and up sphere centers have z -coordinate 0 and $H = \sqrt{3c^2 - d^2}$, respectively. The angle α ($60^\circ \leq \alpha \leq 90^\circ$) is the head angle of the isosceles triangle obtained from the projection on the xy plane of the tilted equilateral triangle the corners of which are the centers of the spheres with coordinates $(\pm c, d, 0)$ and $(0, 0, H)$ such that $c = d \tan(\alpha/2)$, which defines the parameter d .

To compute the 3n-dimensional phase-space volume V_n available to the centers of n spheres free to move, we slightly decrease the density of straight and bent stripes configurations below the close-packing value by reducing the radius c of all spheres by $\delta \ll c$. For angles close to $\alpha = 60^\circ$, to avoid that free up (down) spheres can be confined by the down (up) wall, δ should be small enough. For one sphere free to move this condition is given by: $\delta/c < (1 - \sqrt{1 + \cot^2(\alpha/2)})/2$. The condition $\delta \ll c$ allows to neglect the curvature of the surfaces which define the volume V_n so that it is possible to compute V_n as a 3n-dimensional polytope. For $n = 1$ this can be seen from simple geometric considerations; while $V_1 \sim \delta^3$, the difference between the volume V_1 computed considering curved surfaces and planar surfaces scales as δ^4 and thus may be neglected. This follows considering that the volume V_1 can be computed integrating xy slices along the z direction (see Figs. S1, S2). The perimeter of each slice of the curved polyhedron is composed of arcs specified by the angle $\theta \sim \delta$ and the radius of leading order $2c$ in δ . For each arc, the area of the corresponding segment (the area of a sector minus the triangular piece) is given by $2c^2(\theta - \sin(\theta)) \simeq c^2\theta^3/3 \sim \delta^3$, so that the difference between the area described by the curved and the flat perimeter (indicated in pink in Fig. S1c) is $\sim \delta^3$. Considering the third dimension, z , gives the anticipated result.

The volume V_1 available to the center of one sphere free to move is given by a 2δ -scaled Voronoi cell. The volume V_1 can be computed by integrating xy slices along the z direction (Fig. S2). For the straight stripes configuration, because the symmetry of xy slices under the transformations $x \rightarrow -x$ and $y \rightarrow -y$, we can just compute the area of the slice in one quadrant and multiply it by 4 so that we obtain

$$\begin{aligned}
 V_1^{straight} &= 4 \int_{H-\frac{4c}{H}\delta}^{H-\frac{2c}{H}\delta} dz \int_{\frac{H^2}{c}-\frac{Hz}{c}-4\delta}^0 \left(\frac{c}{d}x - \frac{H^2 - Hz - 4c\delta}{d} \right) dx + 4 \int_{H-\frac{2c}{H}\delta}^{H+\delta} dz \int_{-2\delta}^0 \left(\frac{c}{d}x - \frac{H^2 - Hz - 4c\delta}{d} \right) dx \\
 &= \frac{4c}{d} \left(6 + \frac{H}{c} + \frac{28}{3} \frac{c}{H} \right) \delta^3 = 4 \left(6 \tan\left(\frac{\alpha}{2}\right) + \sqrt{3 \tan^2\left(\frac{\alpha}{2}\right) - 1} + \frac{28 \tan^2\left(\frac{\alpha}{2}\right)}{3\sqrt{3 \tan^2\left(\frac{\alpha}{2}\right) - 1}} \right) \delta^3
 \end{aligned} \tag{S1}$$

From geometric considerations it is possible to see that in the bent stripe configuration, for angles α larger than some threshold value α^* , the sphere centered in $(c, d, 0)$ becomes irrelevant in order to delimit the volume available to the

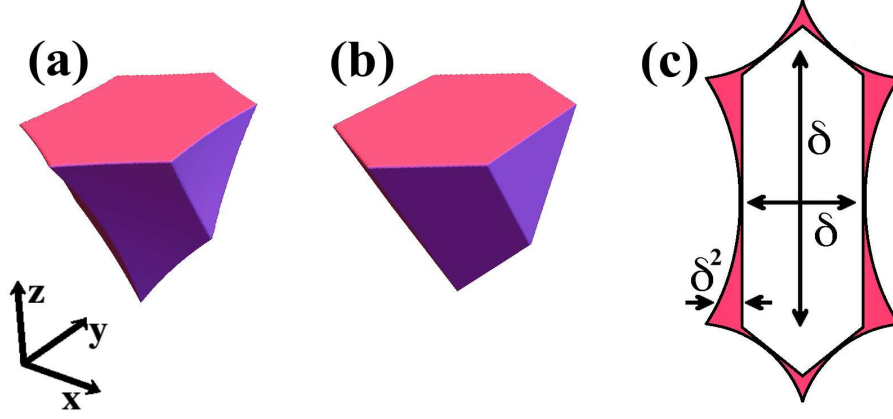


FIG. S1. Phase space volume of one hard sphere free to move in the straight stripe configuration given by the 3-dimensional volume V_1 , considering curved (a) and flat (b) surfaces. Here $\alpha = 70^\circ$ and $\delta/c = 0.08$ to emphasize the difference between curved and flat surfaces. (c) xy slice of the straight stripe free volume which shows the order in δ of the difference between curved and flat areas.

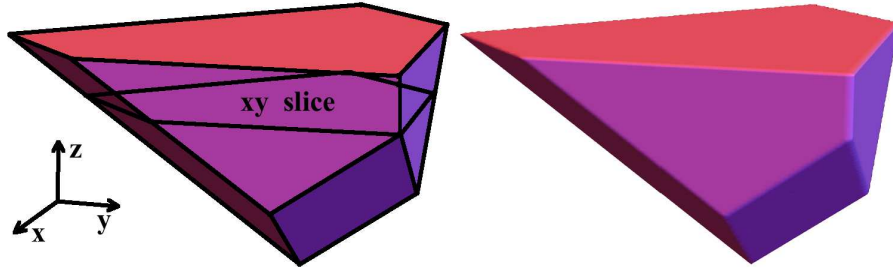


FIG. S2. Phase space volumes of one hard sphere free to move in the bent stripe configuration given by the 3-dimensional volume V_1 , considering flat surfaces. Here $\delta/c = 0.08$, and $\alpha = 90^\circ$, for which the difference between straight and bent stripe volumes is maximal. The left panel is a reproduction of the right one, but in which a xy slice which when integrated along the z axis gives V_1 is indicated.

free sphere for $z > z^*$ with $z^* = H + 2(d^2 - c^2)\delta/(cH)$. Therefore, α^* corresponds to the extreme case in which the previous inequality becomes an equality, that is for $z = H + \delta$

$$H + \delta = H + 2(d^2 - c^2)\delta/(cH) \quad (\text{S2})$$

that can be written as

$$7 \cot^2 \left(\frac{\alpha^*}{2} \right) - 4 \cot^4 \left(\frac{\alpha^*}{2} \right) - 1 = 0 \quad (\text{S3})$$

hence

$$\alpha^* = 2 \arctan \left(\sqrt{\frac{8}{7 + \sqrt{33}}} \right) \simeq 77^\circ \quad (\text{S4})$$

The contributions to the volume V_1^{bent} coming from angles $\alpha < \alpha^*$ and $\alpha > \alpha^*$ have to be computed separately because the xy slices to be integrated along the z axis are described by polygons with a different number of edges

(see Fig. S2). So that we have

$$\begin{aligned}
V_1^{bent}(\alpha < \alpha^*) &= \int_{H-\frac{4c}{H}\delta}^{H-\frac{2c}{H}\delta} dz \left[\int_{-\frac{2cH}{c^2+d^2}(z-H+\frac{4c}{H}\delta)}^{\frac{H(c^2-d^2)}{c(c^2+d^2)}(z-H+\frac{4c}{H}\delta)} \left(\frac{c(3d^2-c^2)}{dH^2}x + \frac{(c^2+d^2)}{dH}z + \frac{(c^2+d^2)(4c\delta-H^2)}{dH^2} \right) dx \right. \\
&\quad + \left. \int_{\frac{H(c^2-d^2)}{c(c^2+d^2)}(z-H+\frac{4c}{H}\delta)}^{4\delta+\frac{H}{c}z-\frac{H^2}{c}} \frac{1}{d}(-x+Hz-H^2+4c\delta)dx \right] + \int_{H-\frac{2c}{H}\delta}^{H+\delta} dz \left[\int_{-\frac{2cH}{c^2+d^2}(z-H+\frac{4c}{H}\delta)}^{-\frac{2cH}{c^2+d^2}(z-H+\frac{c^2+d^2}{cH}\delta)} \right. \\
&\quad \left. \left(\frac{c(3d^2-c^2)}{dH^2}x + \frac{(c^2+d^2)}{dH}z + \frac{(c^2+d^2)(4c\delta-H^2)}{dH^2} \right) dx + \int_{-\frac{2cH}{c^2+d^2}(z-H+\frac{c^2+d^2}{cH}\delta)}^{\frac{2cH}{c^2+d^2}(z-H+\frac{H}{c}\delta)} \right. \\
&\quad \left. \frac{1}{2cd}((d^2-c^2)x+2(c^2+d^2)\delta)dx + \int_{\frac{2cH}{c^2+d^2}(z-H+\frac{H}{c}\delta)}^{2\delta} \frac{1}{d}(-cx+Hz-H^2+4c\delta)dx \right] \\
&\quad - \int_{H-\frac{4c}{H}\delta}^{H+\delta} dz \int_{-\frac{2cH}{c^2+d^2}(z-H+\frac{4c}{H}\delta)}^0 \frac{1}{d}(-cx-Hz+H^2-4c\delta)dx + \frac{1}{4}V_1^{straight} \\
&= \frac{4c}{d} \left(6 + \frac{H}{c} + \frac{28}{3} \frac{c}{H} \right) \delta^3 \equiv V_1^{straight}
\end{aligned} \tag{S5}$$

and

$$\begin{aligned}
V_1^{bent}(\alpha > \alpha^*) &= \int_{H-\frac{4c}{H}\delta}^{H-\frac{2c}{H}\delta} dz \left[\int_{-\frac{2cH}{c^2+d^2}(z-H+\frac{4c}{H}\delta)}^{\frac{H(c^2-d^2)}{c(c^2+d^2)}(z-H+\frac{4c}{H}\delta)} \left(\frac{c(3d^2-c^2)}{dH^2}x + \frac{(c^2+d^2)}{dH}z + \frac{(c^2+d^2)(4c\delta-H^2)}{dH^2} \right) dx \right. \\
&\quad + \left. \int_{\frac{H(c^2-d^2)}{c(c^2+d^2)}(z-H+\frac{4c}{H}\delta)}^{4\delta+\frac{H}{c}z-\frac{H^2}{c}} \frac{1}{d}(-cx+Hz-H^2+4c\delta)dx \right] + \int_{H-\frac{2c}{H}\delta}^{H+\delta} dz \int_{-\frac{2cH}{c^2+d^2}(z-H+\frac{c^2+d^2}{cH}\delta)}^{-\frac{2cH}{c^2+d^2}(z-H+\frac{4c}{H}\delta)} \\
&\quad \left(\frac{c(3d^2-c^2)}{dH^2}x + \frac{(c^2+d^2)}{dH}z + \frac{(c^2+d^2)(4c\delta-H^2)}{dH^2} \right) dx \\
&\quad + \int_{H-\frac{2c}{H}\delta}^{H+\frac{2(d^2-c^2)}{dH}\delta} dz \left[\int_{-\frac{2cH}{c^2+d^2}(z-H+\frac{c^2+d^2}{cH}\delta)}^{\frac{2cH}{c^2+d^2}(z-H+\frac{H}{c}\delta)} \frac{1}{2cd}((d^2-c^2)x+2(c^2+d^2)\delta)dx \right. \\
&\quad + \left. \int_{\frac{2cH}{c^2+d^2}(z-H+\frac{H}{c}\delta)}^{2\delta} \frac{1}{d}(-cx+Hz-H^2+4c\delta)dx \right] + \int_{H+\frac{2(d^2-c^2)}{dH}\delta}^{H+\delta} dz \int_{-\frac{2cH}{c^2+d^2}(z-H+\frac{c^2+d^2}{cH}\delta)}^{2\delta} \\
&\quad \frac{1}{2cd}((d^2-c^2)x+2(c^2+d^2)\delta)dx - \int_{H-\frac{4c}{H}\delta}^{H+\delta} dz \int_{-\frac{2cH}{c^2+d^2}(z-H+\frac{4c}{H}\delta)}^0 \frac{1}{d}(-cx-Hz+H^2-4c\delta)dx \\
&\quad + \frac{1}{4}V_1^{straight} = \frac{\delta^3}{3c^2dH(c^2+d^2)} \left[174c^6 + 88c^4d^2 + 18c^2d^4 - 8d^6 + H(87c^5 + 47c^3d^2 + 12cd^4) \right].
\end{aligned} \tag{S6}$$

In Fig. S3 we show the volumes $V_1^{straight}$ and V_1^{bent} of one sphere free to move for straight and bent stripes configurations, respectively, rescaled by δ^3 for several values of the deformation angles α .

To compute the volume of high dimensional polytopes we use a modified version of the Lasserre method [28, 29] implemented in the VINCI code [30]. Lasserre's method is a signed decomposition method which uses a half space representation to describe each polytope. The modified version implemented in [30] incorporates a detection method

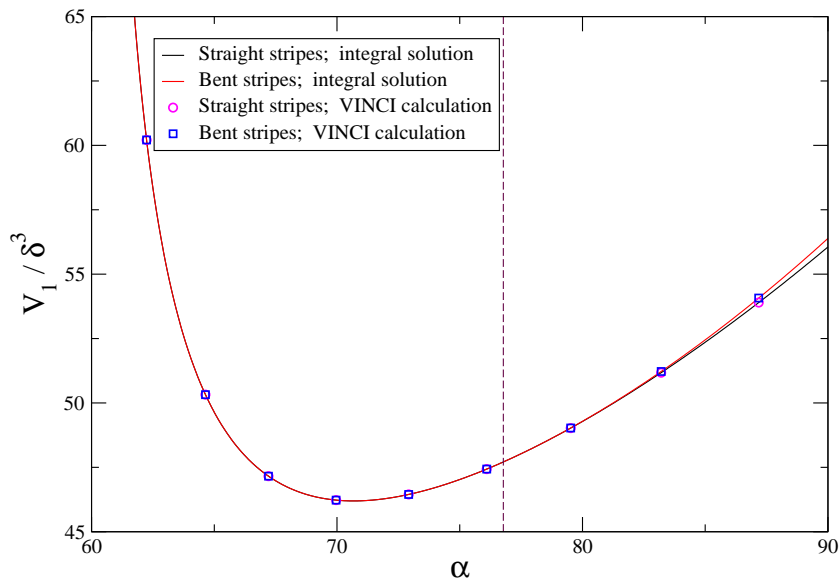


FIG. S3. The volume rescaled by δ^3 available to the center of one sphere free to move in the straight ($V_1^{straight}/\delta^3$) and bent (V_1^{bent}/δ^3) stripes configurations. The vertical dashed line corresponds to the threshold angle $\alpha^* \approx 77^\circ$.

of simplicial faces and a storing/reusing scheme for face volumes which can make a big use of computer memory (which increases exponentially with the system size saturating the 384 GB of RAM of the computer we used already for $n = 5$, and forcing to use slow swap memory for $n = 6$) improving the efficiency of the original algorithm.

In Fig. S3 we compare the analytic expression of volumes $V_1^{straight}$ and V_1^{bent} we obtained from direct integration in Eqs. (S5,S6) with points we get from the VINCI code. From it we can see that the VINCI code is properly implemented in our code and that for $\alpha > \alpha^*$ the curves corresponding to straight and bent stripes split.

SIII. Soft potential model

We consider the ground state configurations given by straight and bent stripes in the soft potential model given by U (harmonic potential), U_r (repulsive harmonic potential) and U_r^γ (repulsive power-law potential). The mechanical equilibrium position of particles are given by $\{x_i, y_i, z_i\}$, and the displacement about these positions are $\{u_i, v_i, w_i\}$. We consider small displacement around mechanical equilibria. The distance between particles i and j is given by

$$dr^2 = (dx + du)^2 + (dy + dv)^2 + (dz + dw)^2 = dr_0^2 + 2(dxdu + dydv + dzdw) + du^2 + dv^2 + dw^2 \quad (S7)$$

where $dx = x_i - x_j$, $dy = y_i - y_j$, $dz = z_i - z_j$, $du = u_i - u_j$, $dv = v_i - v_j$, $dw = w_i - w_j$, and $dr_0 = (dx^2 + dy^2 + dz^2)^{1/2} = 2c$ is the equilibrium separation between the particles. Ignoring the linear terms in du , dv and dw because we will expand around mechanical equilibria (as in ref. [20]), we write

$$dr^2 = dr_0^2 + du^2 + dv^2 + dw^2 \quad (S8)$$

Because terms in the harmonic expansion of the Hamiltonian contain also terms linear in dr , we take the square root of Eq. (S7) and expand to harmonic order

$$dr = dr_0 + \frac{du^2}{2dr_0} \left(1 - \frac{dx^2}{dr_0^2}\right) + \frac{dv^2}{2dr_0} \left(1 - \frac{dy^2}{dr_0^2}\right) + \frac{dw^2}{2dr_0} \left(1 - \frac{dz^2}{dr_0^2}\right) - \frac{dx dy du dv}{dr_0^3} - \frac{dx dz du dw}{dr_0^3} - \frac{dy dz dv dw}{dr_0^3} \quad (S9)$$

The Hamiltonians \mathcal{H} , \mathcal{H}_r and \mathcal{H}_r^γ associated to the potentials U , U_r and U_r^γ respectively, are defined as

$$\begin{cases} \mathcal{H} &= U_0 \sum_{m,n,p} \sum_l \zeta_l^2 \\ \mathcal{H}_r &= U_0 \sum_{m,n,p} \sum_l \zeta_l^2 \cdot \theta(\zeta_l) \\ \mathcal{H}_r^\gamma &= U_0 \sum_{m,n,p} \sum_l \zeta_l^\gamma \cdot \theta(\zeta_l) \end{cases} \quad (S10)$$

where $\zeta_l = (dr_0 - dr_l)/(2\delta)$. The usual sum over nearest-neighbor pairs $\langle i, j, k \rangle$ is here replaced by all particles (m, n, p) and the label l is associated to the additional sum over the neighbors each particle has. The range of values over which

these sums are performed is specified in the next sections for straight and bent configurations. There we consider the Hamiltonian \mathcal{H} for which the exact result of the associated entropy can be written following the approach specified for the Ising model in the main text in Eqs. (1,2). In particular, we compute the associated matrix A for a specific set of 1, 2 and 3 particles free to move according to its definition as: $\mathcal{H} = U_0/(4\delta^2) \sum_{m,n} A_{m,n} q_m q_n$ where K is replaced by $U_0/(4\delta^2)$. We obtain the entropy of straight and bent stripes configurations associated to the Hamiltonian \mathcal{H}_r and \mathcal{H}_r^γ by directly integrating the related partition function.

Straight Stripes

Performing the sum over the index $l = 1, 2, 3, 4, 5, 6$ associated to the six neighbors of the central particle, we obtain (up to additive constants)

$$\mathcal{H} = \frac{U_0}{4\delta^2} \sum_{m,n,p} \left\{ -4c(dr_1 + dr_2 + dr_3 + dr_4 + dr_5 + dr_6) + (dr_1^2 + dr_2^2 + dr_3^2 + dr_4^2 + dr_5^2 + dr_6^2) \right\} + \mathcal{H}_{wall} \quad (\text{S11})$$

where \mathcal{H}_{wall} is the contribution to the Hamiltonian coming from the interaction of the central particle with the wall. The indices and positions at mechanical equilibrium of the central particle and its six neighbors are given in Table S1 in which $c = d \tan(\alpha/2)$ with $60^\circ < \alpha < 90^\circ$ and $H = \sqrt{3c^2 - d^2}$ with $0 < H < \sqrt{2}c$.

l	index	x	y	z
0	(m,n,p)	0	0	H
1	(m+1,n,p)	2c	0	H
2	(m+1,n+1,p-1)	c	d	0
3	(m-1,n+1,p-1)	-c	d	0
4	(m-1,n,p)	-2c	0	H
5	(m-1,n-1,p-1)	-c	-d	0
6	(m+1,n-1,p-1)	c	-d	0

particles	dx	dy	dz
1,0	2c	0	0
2,0	c	d	-H
3,0	-c	d	-H
4,0	-2c	0	0
5,0	-c	-d	-H
6,0	c	-d	-H

TABLE S1. Indices and positions of the central particle 0 and his six neighbours $l = 1, \dots, 6$ (left) and distances between the neighbouring particles and the central one (right) in the unit cell of the straight stripe configuration.

Using Eqs. (S8, S9) and the position of particles in Table S1, noting that $du_l = u_l - u_0$, $dv_l = v_l - v_0$ and $dw_l = w_l - w_0$, and absorbing the terms with indices $l = 4, 5, 6$ in the terms with indices $l = 1, 2, 3$, we can rewrite Eq. (S11) as

$$\begin{aligned} \mathcal{H} = & \frac{U_0}{2\delta^2} \sum_{m,n,p} \left\{ \frac{3}{2}u_0^2 - u_0u_1 - \frac{1}{4}(u_0u_2 + u_0u_3) - \frac{d}{4c}(u_0v_2 + u_2v_0 - u_0v_3 - u_3v_0) \right. \\ & + \frac{H}{4c} \text{sign}(dz_0 - H/2)(u_0w_2 - u_0w_3 + u_2w_0 - u_3w_0) + \frac{d^2}{2c^2}v_0^2 \\ & - \frac{d^2}{4c^2}(v_0v_2 + v_0v_3) + \frac{Hd}{4c^2} \text{sign}(dz_0 - H/2)(v_0w_2 + v_2w_0 + v_0w_3 + v_3w_0) \\ & \left. + \left(2 - \frac{d^2}{2c^2} \right) w_0^2 - \frac{H^2}{4c^2}(w_0w_2 + w_0w_3) \right\} \end{aligned} \quad (\text{S12})$$

where $\text{sign}(\cdot)$ is the usual sign function and it takes into account the fact that the sign of the contributions to the Hamiltonian coming from combination of variables $u_i w_j$ and $v_i w_j$ depends on the particle 0 being up or down. In the previous expression of the Hamiltonian, we considered the contribution of the interaction with the wall given by $\mathcal{H}_{wall} = U_0 w_0^2 dz_{wall}^2 / (16c^2 \delta^2)$ with $dz_{wall} = 2c$. For bent configuration the contribution of \mathcal{H}_{wall} is the same as for the straight configuration. In the following we specify the expression of the matrix A for 1, 2 and 3 particles free to move, A_s^0 , A_s^{01} and A_s^{012} respectively, where the subscript s stays for straight and the superscript indicates the

particles as specified in Table S1, which are free to move.

$$A_s^0 = \begin{pmatrix} 3 & 0 & 0 \\ 0 & \frac{d^2}{c^2} & 0 \\ 0 & 0 & 4 - \frac{d^2}{c^2} \end{pmatrix} \quad (\text{S13})$$

$$A_s^{01} = \begin{pmatrix} 3 & 0 & 0 & -1 & 0 & 0 \\ 0 & \frac{d^2}{c^2} & 0 & 0 & 0 & 0 \\ 0 & 0 & 4 - \frac{d^2}{c^2} & 0 & 0 & 0 \\ -1 & 0 & 0 & 3 & 0 & 0 \\ 0 & 0 & 0 & 0 & \frac{d^2}{c^2} & 0 \\ 0 & 0 & 0 & 0 & 0 & 4 - \frac{d^2}{c^2} \end{pmatrix} \quad (\text{S14})$$

$$A_s^{012} = \begin{pmatrix} 3 & 0 & 0 & -1 & 0 & 0 & -\frac{1}{4} & -\frac{d}{4c} & \frac{H}{4c} \\ 0 & \frac{d^2}{c^2} & 0 & 0 & 0 & 0 & -\frac{d}{4c} & -\frac{d^2}{4c^2} & \frac{dH}{4c^2} \\ 0 & 0 & 4 - \frac{d^2}{c^2} & 0 & 0 & 0 & \frac{H}{4c} & \frac{dH}{4c^2} & -\frac{H^2}{4c^2} \\ -1 & 0 & 0 & 3 & 0 & 0 & -\frac{1}{4} & \frac{d}{4c} & -\frac{H}{4c} \\ 0 & 0 & 0 & 0 & \frac{d^2}{c^2} & 0 & \frac{d}{4c} & -\frac{d^2}{4c^2} & \frac{dH}{4c^2} \\ 0 & 0 & 0 & 0 & 0 & 4 - \frac{d^2}{c^2} & -\frac{H}{4c} & \frac{dH}{4c^2} & -\frac{H^2}{4c^2} \\ -\frac{1}{4} & -\frac{d}{4c} & \frac{H}{4c} & -\frac{1}{4} & \frac{d}{4c} & -\frac{H}{4c} & 3 & 0 & 0 \\ -\frac{d}{4c} & -\frac{d^2}{4c^2} & \frac{dH}{4c^2} & \frac{d}{4c} & -\frac{d^2}{4c^2} & \frac{dH}{4c^2} & 0 & \frac{d^2}{c^2} & 0 \\ \frac{H}{4c} & \frac{dH}{4c^2} & -\frac{H^2}{4c^2} & -\frac{H}{4c} & \frac{dH}{4c^2} & -\frac{H^2}{4c^2} & 0 & 0 & 4 - \frac{d^2}{c^2} \end{pmatrix} \quad (\text{S15})$$

Bent Stripes

Here we compute the Hamiltonian of the ground state consisting of maximally-zigzagging stripes. It has a unit cell of two particles, 0 and 1, and we set the position of particle 0 as the origin and the x -direction to run along the line

connecting particles 0 and 1. Particle 0 represents the particles with odd m , and particle 1 represents the particles with even m , hence we set for particle 0, $m = 2t - 1$, and for particle 1, $m = 2t$, where $1 \leq t \leq L/2$. The positions of the two particles in the unit cell and their 8 neighbors are listed in Table S2.

l	index	x	y	z	particles	dx	dy	dz
0	(m,n,p)	0	0	H	1,0	$2c$	0	0
1	(m+1,n,p)	$2c$	0	H	4,0	c	d	-H
2	(m+2,n,p-1)	$2c + c \frac{3d^2 - c^2}{c^2 + d^2}$	$-d \frac{H^2}{c^2 + d^2}$	0	5,0	$2c \frac{c^2 - d^2}{c^2 + d^2}$	$\frac{4c^2 d}{c^2 + d^2}$	0
3	(m+2,n+1,p-1)	$2c + c$	d	0	6,0	$-c \frac{3d^2 - c^2}{c^2 + d^2}$	$d \frac{H^2}{c^2 + d^2}$	-H
4	(m+1,n+1,p-1)	c	d	0	7,0	$-c$	$-d$	-H
5	(m-1,n+1,p)	$2c \frac{c^2 - d^2}{c^2 + d^2}$	$\frac{4c^2 d}{c^2 + d^2}$	H	8,0	c	$-d$	-H
6	(m-1,n,p-1)	$-c \frac{3d^2 - c^2}{c^2 + d^2}$	$d \frac{H^2}{c^2 + d^2}$	0	2,1	$c \frac{3d^2 - c^2}{c^2 + d^2}$	$-d \frac{H^2}{c^2 + d^2}$	-H
7	(m-1,n-1,p-1)	$-c$	$-d$	0	3,1	c	d	-H
8	(m+1,n-1,p-1)	c	$-d$	0	4,1	$-c$	d	-H
9	(m+2,n-1,p)	$2c - 2c \frac{c^2 - d^2}{c^2 + d^2}$	$-\frac{4c^2 d}{c^2 + d^2}$	H	8,1	$-c$	$-d$	-H
					9,1	$-2c \frac{c^2 - d^2}{c^2 + d^2}$	$-\frac{4c^2 d}{c^2 + d^2}$	0

TABLE S2. Indices and positions of the particles 0 and 1 and their eight neighbours $l = 2, \dots, 9$ (left) and distances between the neighbouring particles and 0 and 1 particles (right) in the unit cell of the maximally zigzagging stripe configuration.

The Hamiltonian is

$$\mathcal{H} = \frac{U_0}{4\delta^2} \sum_{t,n,p} \left\{ -4c(dr_{10} + dr_{40} + dr_{50} + dr_{60} + dr_{70} + dr_{80} + dr_{21} + dr_{31} + dr_{41} + dr_{81} + dr_{91}) \right. \\ \left. + (dr_{10}^2 + dr_{40}^2 + dr_{50}^2 + dr_{60}^2 + dr_{70}^2 + dr_{80}^2 + dr_{21}^2 + dr_{31}^2 + dr_{41}^2 + dr_{81}^2 + dr_{91}^2) \right\} + \mathcal{H}_{wall} \quad (\text{S16})$$

Absorbing the terms with indices 60, 70, 80, 01, 81, 91 in the terms with indices 10, 40, 50, 21, 31, 41, the Hamiltonian becomes

$$\mathcal{H} = \frac{U_0}{2\delta^2} \sum_{t,n,p} \left\{ \frac{3c^4 + 5d^4}{2(c^2 + d^2)^2} (u_0^2 + u_1^2) - u_0 u_1 - \frac{1}{4} (u_0 u_4 + u_1 u_3) + \frac{4c^2 d^2}{(c^2 + d^2)^2} u_0 u_5 \right. \\ \left. + \frac{d(3c^4 - 4c^2 d^2 + d^4)}{c(c^2 + d^2)^2} (u_0 v_0 + u_1 v_1) - \frac{d}{4c} (u_0 v_4 + u_1 v_3 - u_1 v_4 + u_3 v_1 + u_4 v_0 - u_4 v_1) \right. \\ \left. - \frac{2cd(c^2 - d^2)}{(c^2 + d^2)^2} (u_0 v_5 + u_5 v_0) + \frac{(-c^4 + 6c^2 d^2 - 9d^4)}{4(c^2 + d^2)^2} u_1 u_2 + \frac{d(3d^2 - c^2)(3c^2 - d^2)}{4c(c^2 + d^2)^2} \right. \\ \left. \cdot (u_1 v_2 + u_2 v_1) + \frac{H}{4c} \text{sign}(dz_0 - H/2) (u_0 w_4 + u_1 w_3 - u_1 w_4 + u_3 w_1 + u_4 w_0 - u_4 w_1) \right. \\ \left. + \frac{H(3d^2 - c^2)}{4c(c^2 + d^2)} \text{sign}(dz_0 - H/2) (u_1 w_2 + u_2 w_1) + \frac{d^2(7c^4 + d^4)}{2c^2(c^2 + d^2)^2} (v_0^2 + v_1^2) \right. \\ \left. - \frac{d^2}{4c^2} (v_0 v_4 + v_1 v_3 + v_1 v_4) - \frac{4c^2 d^2}{(c^2 + d^2)^2} v_0 v_5 + \frac{d^2(-9c^4 + 6c^2 d^2 - d^4)}{4c^2(c^2 + d^2)^2} v_1 v_2 \right. \\ \left. + \frac{Hd}{4c^2} \text{sign}(dz_0 - H/2) (v_0 w_4 + v_1 w_3 + v_1 w_4 + v_3 w_1 + v_4 w_0 + v_4 w_1) \right. \\ \left. - \frac{Hd(3c^2 - d^2)}{4c^2(c^2 + d^2)} \text{sign}(dz_0 - H/2) (v_1 w_2 + v_2 w_1) + \left(2 - \frac{d^2}{2c^2}\right) (w_0^2 + w_1^2) \right. \\ \left. - \frac{H^2}{4c^2} (w_0 w_4 + w_1 w_2 + w_1 w_3 + w_1 w_4) \right\} \quad (\text{S17})$$

In the following we specify the expression of the matrix A for 1,2 and 3 particles free to move, A_b^0, A_b^{01} and A_b^{014} respectively, where the subscript b stays for bent and the superscript indicates the particles as specified in Table S2, which are free to move.

$$A_b^0 = \begin{pmatrix} A_{11} & A_{12} & A_{13} \\ A_{12} & A_{22} & A_{23} \\ A_{13} & A_{23} & A_{33} \end{pmatrix} \quad (\text{S18})$$

$$A_b^{01} = \begin{pmatrix} A_{11} & A_{12} & A_{13} & -1 & 0 & 0 \\ A_{12} & A_{22} & A_{23} & 0 & 0 & 0 \\ A_{13} & A_{23} & A_{33} & 0 & 0 & 0 \\ -1 & 0 & 0 & A_{11} & A_{12} & -A_{13} \\ 0 & 0 & 0 & A_{12} & A_{22} & -A_{23} \\ 0 & 0 & 0 & -A_{13} & -A_{23} & A_{33} \end{pmatrix} \quad (\text{S19})$$

$$A_b^{012} = \begin{pmatrix} A_{11} & A_{12} & A_{13} & -1 & 0 & 0 & -\frac{1}{4} & A_{18} & A_{19} \\ A_{12} & A_{22} & A_{23} & 0 & 0 & 0 & A_{18} & A_{28} & A_{29} \\ A_{13} & A_{23} & A_{33} & 0 & 0 & 0 & A_{19} & A_{29} & A_{39} \\ -1 & 0 & 0 & A_{11} & A_{12} & -A_{13} & -\frac{1}{4} & -A_{18} & -A_{19} \\ 0 & 0 & 0 & A_{12} & A_{22} & -A_{23} & -A_{18} & A_{29} & A_{29} \\ 0 & 0 & 0 & -A_{13} & -A_{23} & A_{33} & -A_{19} & A_{29} & A_{39} \\ -\frac{1}{4} & A_{18} & A_{19} & -\frac{1}{4} & -A_{18} & -A_{19} & A_{11} & A_{12} & -A_{13} \\ A_{18} & A_{28} & A_{29} & -A_{18} & A_{28} & A_{29} & A_{12} & A_{22} & -A_{23} \\ A_{19} & A_{29} & A_{39} & -A_{19} & A_{29} & A_{39} & -A_{13} & -A_{23} & A_{33} \end{pmatrix} \quad (\text{S20})$$

The elements of matrices A_b^0, A_b^{01} and A_b^{014} are specified in the following

$$\left\{ \begin{array}{l} A_{11} = \frac{3c^4 + 5d^4}{(c^2 + d^2)^2} \\ A_{12} = \frac{d(c^2 - d^2)H^2}{c(c^2 + d^2)^2} \\ A_{13} = \frac{(d^2 - c^2)H}{2c(c^2 + d^2)} \\ A_{18} = -\frac{d}{4c} \\ A_{19} = \frac{H}{4c} \end{array} \right. \left\{ \begin{array}{l} A_{22} = \frac{d^2(7c^4 + d^4)}{c^2(c^2 + d^2)^2} \\ A_{23} = \frac{d(d^2 - c^2)H}{2c^2(c^2 + d^2)} \\ A_{33} = 4 - \frac{d^2}{c^2} \\ A_{28} = -\frac{d^2}{4c^2} \\ A_{29} = \frac{dH}{4c^2} \\ A_{39} = -\frac{H^2}{4c^2} \end{array} \right. \quad (\text{S21})$$

Using the expression for the entropy in Eq.(2), we can obtain the entropy difference per particle between straight and bent configurations: $\Delta s = 1/n \cdot \log(\|A_b\|/\|A_s\|)$, as shown in Fig. 4a for 1, 2 and 3 particles free to move.

SIII. Soft spheres interacting through the square-shoulder repulsive potential

One of the simplest soft potentials close to the hard-sphere model is the square-shoulder repulsive potential which describes particles with a hard core surrounded by a soft corona. This model can have a very rich behavior and it has been shown to develop pattern formation [48], different mesophases [49] and quasi-crystals [50]. In the case of one sphere free to move, the entropy of such soft spheres system in the canonical ensemble can be evaluated through the partition function assuming the following soft inter-particle potential

$$\phi_{soft}(r) = \begin{cases} \infty & \text{for } r \leq a_H \\ \phi_0 & \text{for } a_H < r \leq a_S \\ 0 & \text{for } r > a_S \end{cases} \quad (\text{S22})$$

where a_H and a_S are the hard and soft radii respectively, and ϕ_0 is the soft potential strength. In computing the partition function one can split the integral on the coordinate r of the center of the free sphere to the following three regions: $|r - r_i| \leq a_H$, $a_H < |r - r_i| < a_S$ and $|r - r_i| \geq a_S$ for all r_i where r_i are the coordinates of the six spheres and the wall which confine the free sphere. The integral on the first region does not contribute to the partition function while the integrals on the second and third regions contribute the terms $e^{-\beta\phi_0}\Delta V_{1,\rho_H,\rho_S}$ and V_{1,ρ_S} respectively, where $\rho_{H,S} = (4/3)\pi a_{H,S}^3 N/V_0$ and $\Delta V_{1,\rho_H,\rho_S} = V_{1,\rho_H} - V_{1,\rho_S}$. Using the expression of the entropy in the left-hand side of Eq. (2) we obtain

$$S_{1,\rho_H,\rho_S}^{soft} = \frac{\beta\phi_0 e^{-\beta\phi_0} \Delta V_{1,\rho_H,\rho_S}}{V_{1,\rho_S} + e^{-\beta\phi_0} \Delta V_{1,\rho_H,\rho_S}} + \ln(V_{1,\rho_S} + e^{-\beta\phi_0} \Delta V_{1,\rho_H,\rho_S}). \quad (\text{S23})$$

The thermal factor, which for soft spheres couples with space variables, is $0 < e^{-\beta\phi_0} < 1$. Because $V_{1,\rho_S}^{bent} > V_{1,\rho_S}^{straight}$ and $\Delta V_{1,\rho_H,\rho_S}^{bent} > \Delta V_{1,\rho_H,\rho_S}^{straight}$, we have that $S_{1,\rho_H,\rho_S}^{soft, bent} > S_{1,\rho_H,\rho_S}^{soft, straight}$ so that bent stripes are still favored with respect to straight stripes in the case of one sphere free to move interacting through a soft-shoulder potential. In the general case of n free spheres, the computation of $S_{n,\rho_H,\rho_S}^{soft}$ is complicated due to the presence of series of powers of ϕ_0 , but, as for the hard-spheres model, we expect that increasing n will not change the preference for bent stripes with respect to straight stripes.

SIV. Asymmetric potential

As an asymmetric potential we first consider the generalized repulsive potential $U_r^\gamma(\zeta) = U_r^0 \zeta^\gamma \cdot \theta(\zeta)$ which reduces to the repulsive harmonic potential for $\gamma = 2$ and gives hard spheres of diameter $2(c - \delta)$ for $\gamma \rightarrow \infty$. U_r^γ differs by a

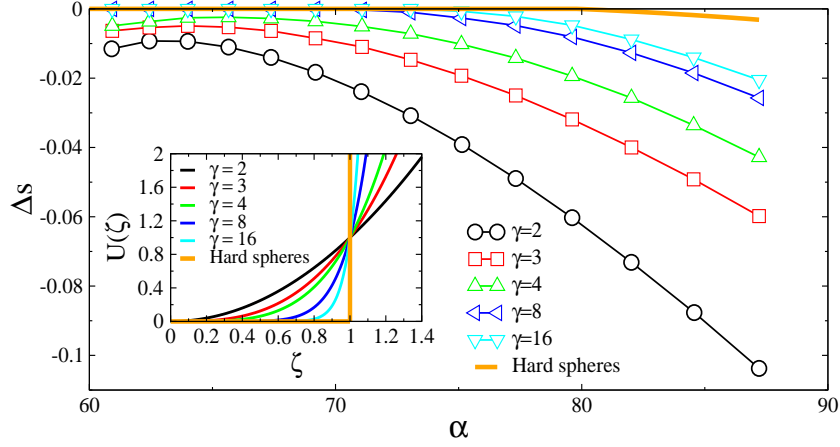


FIG. S4. Entropy difference per particle $\Delta s = \Delta S/n$ between straight and bent stripes configurations for $n = 1$ for the generalized repulsive harmonic potential $U_r^\gamma(\zeta)$. Inset: $U_r^\gamma(\zeta)$.

numerical prefactor from the commonly-used tunable soft repulsive potential [41, 51, 52], with $dr_0 = \sigma_{ij}$ and $dr = r_{ij}$, and the hard-sphere limit obtained for $\alpha \rightarrow 0$ [51]. Figure S4 shows how as γ increases, Δs for one particle free to move slowly approaches the hard-sphere result and always exhibits a preference for bent stripes.

Now we consider the more general asymmetric power-law potential: $U_{asy}(\zeta) = U_r^0 \zeta^{\gamma_r} \theta(\zeta) + U_a^0 (-\zeta)^{\gamma_a} \theta(-\zeta)$ where $\zeta = (dr_0 - dr)/(2\delta)$, with U_r^0 , U_a^0 , γ_r , γ_a constants. The subscripts r and a denote repulsive and attractive respectively. In principle, at finite T , we should compare the free energy of the competing configurations to establish the thermodynamically stable phase. If the Hamiltonian of the system includes only quadratic terms in the canonical variables, as for the deformable antiferromagnetic Ising model or particles interacting through the harmonic potential, the internal energy of straight and bent configurations is the same, as follows from the equipartition theorem, and the difference in the free energy comes only from entropy. For finite T , the internal energy with the asymmetric potential U_{asy} , for which we can not apply the equipartition theorem, could grow differently with temperature for fluctuations around different ground-state configurations. In the following we will show that to establish which is the more stable configuration for particles interacting through U_{asy} , we can compare just the entropy because for small T the internal energy of the different configurations is the same, as for the harmonic potential.

For a harmonic system the equipartition theorem leads to the result that each degree of freedom contributes $\frac{1}{2}kT$ to the internal energy. For anharmonic potentials, as U_{asy} , it is not obvious that the energy grows with T exactly in the same functional form for all competing ground-state configurations. To check this for U_{asy} , we start by considering a simple example of a one-dimensional asymmetric power-law potential of the form

$$U(x) = \begin{cases} U_a^0 (-x)^{\gamma_a} & x < 0 \\ U_r^0 x^{\gamma_r} & x > 0 \end{cases}. \quad (\text{S24})$$

Its canonical partition function is given by

$$Z = \int_{-\infty}^{\infty} \exp[-\beta U(x)] dx = \int_{-\infty}^0 \exp[-\beta U_a^0 (-x)^{\gamma_a}] dx + \int_0^{\infty} \exp[-\beta U_r^0 x^{\gamma_r}] dx. \quad (\text{S25})$$

By change of variables we see that this may be written as

$$Z = C(\gamma_a) (\beta U_a^0)^{-1/\gamma_a} + C(\gamma_r) (\beta U_r^0)^{-1/\gamma_r}, \quad (\text{S26})$$

where the prefactors $C(\gamma)$ will be soon shown to be irrelevant.

The internal energy is given by

$$\langle U \rangle = -\frac{1}{Z} \frac{\partial Z}{\partial \beta} = \frac{\frac{C(\gamma_a)}{\gamma_a \beta} (\beta U_a^0)^{-1/\gamma_a} + \frac{C(\gamma_r)}{\gamma_r \beta} (\beta U_r^0)^{-1/\gamma_r}}{C(\gamma_a) (\beta U_a^0)^{-1/\gamma_a} + C(\gamma_r) (\beta U_r^0)^{-1/\gamma_r}}. \quad (\text{S27})$$

where $\langle \rangle$ refers to the canonical ensemble average. We use the convention that Boltzmann's constant is set to unity,

thus substitute $\beta = 1/T$ and write this as

$$\langle U \rangle = \frac{\frac{C(\gamma_a)}{\gamma_a} (U_a^0)^{-1/\gamma_a} T^{1+1/\gamma_a} + \frac{C(\gamma_r)}{\gamma_r} (U_r^0)^{-1/\gamma_r} T^{1+1/\gamma_r}}{C(\gamma_a)(U_a^0)^{-1/\gamma_a} T^{1/\gamma_a} + C(\gamma_r)(U_r^0)^{-1/\gamma_r} T^{1/\gamma_r}}. \quad (\text{S28})$$

Since $\gamma_a, \gamma_r > 1$, as $T \rightarrow 0$, $T^{1/\gamma_a}, T^{1/\gamma_r} \rightarrow 0$. We are interested in the case that $\gamma_a \neq \gamma_r$. We will denote the smaller and larger of these two exponents as $\gamma_1 = \max(\gamma_a, \gamma_r), \gamma_2 = \min(\gamma_a, \gamma_r)$. That is, $\gamma_1 > \gamma_2$. Now, as $T \rightarrow 0$, $T^{1/\gamma_1} \gg T^{1/\gamma_2}$, and thus

$$\langle U \rangle \approx \frac{T}{\gamma_1}. \quad (\text{S29})$$

Namely, in the low-temperature limit, the internal energy grows with increasing temperature in a manner that depends only on the exponent of the stiffer side of the interaction (attractive or repulsive), and does not depend on the prefactors U_a^0, U_r^0 . From the other hand, if we apply the generalised equipartition function to $U(x)$, that is $\langle x \partial U(x) / \partial x \rangle = T$, we obtain the same result for $\langle U \rangle$. If we apply the generalised equipartition function to $U_{asy}(\zeta)$, we can obtain the same relation as for $\langle U \rangle$, but with a different prefactor. In other words, we have that for $U_{asy}(\zeta)$ the only difference in free energy between straight and bent stripes configurations comes from the entropy difference.

If we fix $U_r^0 = U_a^0 = 1$, we find, computing by numerical integration the canonical partition function, that there is a value of $\gamma_a > \gamma_r$ ($\gamma_a = \gamma_r \cdot \kappa(\alpha)$, with $0 < 1/\kappa < 1$) for which $\Delta s < 0$. See Fig. 4.

If we consider the case of $\gamma_r = \gamma_a$ and change only the prefactors U_r^0 and U_a^0 , we do not find a stripe inversion (that is we never find $\Delta s < 0$ for any U_r^0 and U_a^0). This can also be demonstrated by showing that the attractive component of the potential obtained by changing only the prefactor U_a^0 is always bigger than the attractive component obtained by changing only the exponent γ_a with respect to γ_r (even for $\gamma_a/\gamma_r < \kappa$ for which $\Delta s > 0$). Without loss of generality we fix $U_r^0 = 1$ and change U_a^0 . In the calculation of the partition function Z , we have to integrate over a product of exponentials of the form $\exp(-\beta U_r^0 \zeta^{\gamma_r})$ and $\exp[-\beta U_a^0 (-\zeta)^{\gamma_a}]$. Because we consider $T \rightarrow 0$, that is $\beta \rightarrow \infty$, the main contribution to Z comes from small values of ζ . It results that, once we fix the value of U_a^0 , for $\gamma_a/\gamma_r > 1$ there is a value of $\zeta = \zeta_0 = \zeta_0(\gamma_a/\gamma_r) > 0$ such that for $\zeta < \zeta_0$ we have $\zeta_0^{\gamma_a} < U_a^0 \zeta_0^{\gamma_r}$, that is $\zeta_0^{\gamma_a/\gamma_r} < U_a^0$, for any fixed U_a^0 and $\gamma_a/\gamma_r > 1$ (in particular also for $1 < \gamma_a/\gamma_r < \kappa$, that is for a value of γ_a/γ_r that is still too small to cause the inversion of Δs).